Efficient methods of computing interior transmission eigenvalues for the elastic waves

Wei-Chen Chang* Wen-Wei Lin† Jenn-Nan Wang‡

Abstract

We study the interior transmission eigenvalue problem for the elastic wave scattering in this paper. We aim to show the distribution of positive eigenvalues by efficient numerical algorithms. Here the elastic waves are scattered by the perturbations of medium parameters, which include the elasticity tensor $\mathbf{C}$ and the density ρ. Let us denote $(\mathbf{C}_0, \rho_0)$ and $(\mathbf{C}_1, \rho_1)$ the background and the perturbed medium parameters, respectively. We consider two cases of perturbations, $\mathbf{C}_0 = \mathbf{C}_1, \rho_1 \neq \rho_0$ (case 1) and $\mathbf{C}_0 \neq \mathbf{C}_1, \rho_1 = \rho_0$ (case 2). After discretizing the associated PDEs by FEM, we are facing the computation of generalized eigenvalues problems (GEP) with matrices of large size. These GEPs contain huge number of nonphysical zeros (for case 1) or nonphysical infinities (for case 2). In order to locate several hundred positive eigenvalues effectively, we then convert GEPs to suitable quadratic eigenvalues problems (QEP). We then implement a quadratic Jacobi-Davidson method combining with partial locking or partial deflation techniques to compute 500 positive eigenvalues.

Keywords: Interior transmission eigenvalues, elastic waves, generalized eigenvalue problems, quadratic eigenvalue problems, quadratic Jacobi-Davidson method.

1 Introduction

We study the interior transmission eigenvalue problem (ITEP) for the elastic wave scattering in this paper. Our purpose here is to propose an efficient numerical algorithm to compute as many transmission eigenvalues as possible for the time-harmonic elastic waves. Let D be an open bounded domain in $\mathbb{R}^2$ with smooth boundary ∂D. Let $\mathbf{u}(x) = [u_1(x), u_2(x)]^\top$ be the two-dimensional vector representing the displacement vector and its infinitesimal stain tensor be

*Department of Mathematics, National Taiwan University, Taipei 106, Taiwan. Email: d04221003@ntu.edu.tw

†Department of Applied Mathematics, National Chiao Tung University, Hsinchu 300, Taiwan. E-mail: wwlin@math.nctu.edu.tw

‡Institute of Applied Mathematical Sciences, NCTS, National Taiwan University, Taipei, 106, Taiwan. Email: jnwang@math.ntu.edu.tw

given by $\varepsilon(\mathbf{u}) = ((\nabla\mathbf{u})^T + \nabla\mathbf{u})/2$. We consider the linear elasticity, that is, the stress tensor $\sigma(\mathbf{u})$ is defined by $\varepsilon(\mathbf{u})$ via Hook's law:

$$\sigma_{\mathbf{C}}(\mathbf{u}) = \mathbf{C}\varepsilon(\mathbf{u}),$$

where $\mathbf{C}$ is the elasticity tensor. For elasticity, the elasticity tensor $\mathbf{C} = (C_{ijkl})$, $1 \le i, j, k, l \le 2$, is fourth rank tensor satisfying two symmetry properties:

$$\begin{aligned} C_{ijkl} &= C_{klij} \quad \text{(major symmetry)}, \\ C_{ijkl} &= C_{jikl} \quad \text{(minor symmetry)}. \end{aligned} \tag{1}$$

We also require that $\mathbf{C}$ satisfies the strong convexity condition: there exists $\kappa > 0$ such that for any symmetric matrix A

$$\mathbf{C}A : A \ge \kappa |A|^2 \quad \forall\, x \in D, \tag{2}$$

where for two matrices A, B, $A : B = \sum_{ij} a_{ij} b_{ij}$ and $|A|^2 = A : A$. In particular, the elastic body is called isotropic if

$$C_{ijkl} = \lambda \delta_{ij}\delta_{kl} + \mu(\delta_{ik}\delta_{jl} + \delta_{il}\delta_{jk})$$

where μ and λ are called Lamé coefficients. In other words, for isotropic elastic body, the stress-strain relation is given by

$$\sigma_{\mathbf{C}}(\mathbf{u}) = 2\mu\varepsilon(\mathbf{u}) + \lambda \operatorname{tr}(\varepsilon(\mathbf{u}))I = 2\mu\varepsilon(\mathbf{u}) + \lambda \nabla\cdot\mathbf{u} I, \tag{3}$$

where I stands for the identity matrix. The convexity condition (2) is equivalent to

$$\mu(x) > 0, \quad \lambda + \mu > 0. \tag{4}$$

Let $\mathbf{C}_i$, $i = 0, 1$, be two elasticity tensors satisfying (1), (2). Denote $\sigma_{\mathbf{C}_i}$ its associated stress tensor. The ITEP is to find $\omega^2 \in \mathbb{C}$ such that there exists a nontrivial solution $(\mathbf{u}, \mathbf{v}) \in [H^1(D)]^2 \times [H^1(D)]^2$ solving

$$\nabla \cdot \sigma_{\mathbf{C_0}}(\mathbf{u}) + \rho_0 \omega^2 \mathbf{u} = 0 \quad \text{in} \quad D, \tag{5a}$$

$$\nabla \cdot \sigma_{\mathbf{C_1}}(\mathbf{v}) + \rho_1 \omega^2 \mathbf{v} = 0 \quad \text{in} \quad D, \tag{5b}$$

$$\mathbf{u} = \mathbf{v} \quad \text{on} \quad \partial D, \tag{5c}$$

$$\sigma_{\mathbf{C_0}}(\mathbf{u})\nu = \sigma_{\mathbf{C_1}}(\mathbf{v})\nu \quad \text{on} \quad \partial D, \tag{5d}$$

where ρ_0, ρ_1 are density functions and ν is the outer normal of ∂D. Physically, $\sigma_{\mathbf{C_0}}(\mathbf{u})\nu$ (or $\sigma_{\mathbf{C_1}}(\mathbf{v})\nu$) denotes the traction acting on ∂D.

The study of ITEP originates from the validity of some qualitative approaches to the inverse scattering problems in an inhomogeneous medium such as the linear sampling method [13] and the factorization method [22]. To describe its originality, we assume that $\rho_0 = 1$ and $\sigma_{\mathbf{C_0}}$ is the isotropic stress tensor (3) with constant Lamé coefficients λ, μ. Let the incident field $\mathbf{u}_e^{\text{in}}(x)$ with $e = p$ or s be given by

$$\mathbf{u}_p^{\text{in}}(x) = \xi e^{ik_p x\cdot\xi} \quad \text{or} \quad \mathbf{u}_s^{\text{in}}(x) = \xi^{\perp} e^{ik_s x\cdot\xi}$$

with $\xi \in \Omega := \{\|\xi\|_2 = 1\}$ and $k_p := \omega/\sqrt{\lambda+2\mu}$, $k_s := \omega/\sqrt{\mu}$ represent the compressional and the shear wave numbers, respectively. It is easily seen that $\mathbf{u}_e^{\text{in}}$ satisfies the elastic wave equation

$$\nabla \cdot \sigma_{\mathbf{C_0}}(\mathbf{u}_e^{\text{in}}) + \omega^2 \mathbf{u}_e^{\text{in}} = 0 \quad \text{in} \quad \mathbb{R}^2.$$

Suppose that the homogeneous medium is perturbed by a penetrable object D with elasticity parameters $(\mathbf{C}_1, \rho_1)$. Denote $\widetilde{\mathbf{C}} = \mathbf{C}_1\chi_D + \mathbf{C}_0\chi_{\mathbb{R}^2\setminus\bar{D}}$ and $\tilde{\rho} = \rho_1\chi_D + \chi_{\mathbb{R}^2\setminus\bar{D}}$ and the total field $\mathbf{u}_e^{\text{to}}(x) = \mathbf{u}_e^{\text{in}}(x) + \mathbf{u}_e^{\text{sc}}(x)$ solves

$$\nabla \cdot \sigma_{\widetilde{\mathbf{C}}}(\mathbf{u}_e^{\text{to}}) + \tilde{\rho}\omega^2 \mathbf{u}_e^{\text{to}} = 0 \quad \text{in} \quad \mathbb{R}^2.$$

Here, by the Helmhotlz-Hodge decomposition, we can write $\mathbf{u}_e^{\text{sc}}(x) = \mathbf{u}_{ep}^{\text{sc}}(x) + \mathbf{u}_{es}^{\text{sc}}(x)$. The scattered fields $\mathbf{u}_{ep}^{\text{sc}}(x), \mathbf{u}_{es}^{\text{sc}}(x)$ are required to satisfy the following the Kupradze's radiation conditions at $|x| \to \infty$

$$\frac{\partial \mathbf{u}_{ep}^{\text{sc}}}{\partial |x|} - ik_p \mathbf{u}_{ep}^{\text{sc}} = o(|x|^{-1/2}),$$
$$\frac{\partial \mathbf{u}_{es}^{\text{sc}}}{\partial |x|} - ik_s \mathbf{u}_{es}^{\text{sc}} = o(|x|^{-1/2})$$

uniformly in $\hat{x} = x/|x|$. It is well known that every radiating solution $\mathbf{u}_e^{\text{sc}}(x)$ has an asymptotic behavior of the form

$$\mathbf{u}_e^{\text{sc}}(x) = \frac{e^{ik_p|x|}}{\sqrt{|x|}} u_{ep}^{\infty}(\hat{x},\xi)\hat{x} + \frac{e^{ik_s|x|}}{\sqrt{|x|}} u_{es}^{\infty}(\hat{x},\xi)\hat{x}^{\perp} + O(|x|^{-3/2}),$$

where $\mathbf{u}_e^{\infty}(\hat{x},\xi) := (u_{ep}^{\infty}(\hat{x},\xi), u_{es}^{\infty}(\hat{x},\xi))$ is called the far-field pattern. The inverse problem we are interested in is to reconstruct the shape of the penetrable object D by the far-field patterns $\mathbf{u}_p^{\infty}(\hat{x},\xi) = (u_{pp}^{\infty}(\hat{x},\xi), u_{ps}^{\infty}(\hat{x},\xi))$ and $\mathbf{u}_s^{\infty}(\hat{x},\xi) = (u_{sp}^{\infty}(\hat{x},\xi), u_{ss}^{\infty}(\hat{x},\xi))$ for all $\hat{x}, \xi \in \Omega$.

In the linear sampling method and the factorization method, the following far-field operator $\mathbf{F} : [L^2(\Omega)]^2 \to [L^2(\Omega)]^2$ plays an important role

$$(\mathbf{F}\mathbf{g})(\hat{x}) = e^{-i\pi/4} \int_{\Omega} \left(\sqrt{\frac{k_p}{\omega}} \mathbf{u}_p^{\infty}(\hat{x},\xi) g_p(\xi) + \sqrt{\frac{k_p}{\omega}} \mathbf{u}_s^{\infty}(\hat{x},\xi) g_s(\xi) \right) d\xi,$$

where $\mathbf{g}(\xi) = (g_p(\xi), g_s(\xi))$. Due to the superposition principle, the far-field operator is the far-field pattern of the *elastic Herglotz wave function*

$$\mathbf{u}_{\mathbf{g}}(x) := e^{-i\pi/4} \int_{\Omega} \left(\sqrt{\frac{k_p}{\omega}} \xi e^{ik_p x\cdot\xi} g_p(\xi) + \sqrt{\frac{k_p}{\omega}} \xi^{\perp} e^{ik_s x\cdot\xi} g_s(\xi) \right) d\xi.$$

A well-known result is that the far-field operator $\mathbf{F}$ is injective and has a dense range if and only if ω^2 is not an eigenvalue of (5) with eigenfunction $(\mathbf{u}_{\mathbf{g}}, \mathbf{v})$. Roughly speaking, if ω^2 is an eigenvalue of (5) with corresponding eigenfunction $(\mathbf{u}_{\mathbf{g}}, \mathbf{v})$, the penetrable object D is a *non-scattered* object.

The ITEP have recently enjoyed a rapid development in the study of direct/inverse scattering problems for acoustic and electromagnetic waves in inhomogeneous media [6, 7, 8, 9, 14, 15, 16, 23, 29]. We refer to two monographs [5, 24] for the detailed accounts of the ITEP for acoustic and electromagnetic waves. For the investigation of ITEP for the elastic waves, there are a few theoretical results [1, 2, 10, 11, 12]. Especially, in [1], the fundamental questions of existence and discreteness of transmission eigenvalues associated with (5) were established.

The main focus of this work is to develop a numerical method to compute the transmission eigenvalues of (5). For acoustic and electromagnetic waves, some numerical algorithms for computing the transmission eigenvalues were proposed recently. Three finite element methods and a coupled boundary element method were proposed for solving the 2D/3D ITEP [15, 17, 31]. Two iterative methods combining with convergent analysis based on the existence theory of the fourth order reformulation for the transmission eigenvalues in [8] were considered in [30]. A mixed finite element method for the 2D ITEP was suggested in [20] and the corresponding non-Hermitian quadratic eigenvalue problem (QEP) was solved by the classical secant iteration with an adaptive Arnoldi method. The multilevel correction method was used to transform the solution of TEP into a series of solutions corresponding to linear boundary value problems and then solved by the multigrid method [21].

In many cases, we are mainly interested in locating positive transmission eigenvalues. However, for general inhomogeneous media, the desired positive transmission eigenvalues are surrounded by complex ones. We would like to mention that an accurate numerical method, based on a surface integral formulation of the ITEP, for solving corresponding nonlinear eigenvalue problems for many different obstacles in 3D was presented in [25], but, only constant index of refraction and smooth domain can be treated. In [28] (for 2D ITEP) and [18] (for 3D ITEP), the QEP is rewritten as a particular parametrized symmetric definite generalized eigenvalue problem (GEP) for which the eigenvalue curves are arranged in a monotonic order so that the desired curves can be sequentially solved with a new secant-type iteration. In [26, 27], a quadratic Jacobi-Davidson method with nonequivalence deflation is applied to compute a large number of positive eigenvalues of the corresponding QEPs.

As far as we know, there is only one result [19] considering numerical computation of ITEP for the elastic waves. In [19], a numerical method was presented to compute a few smallest positive transmission eigenvalues of (5). The ITEP was reformulated as locating the roots of a nonlinear function whose values are generalized eigenvalues of a series of self-adjoint fourth-order problems. After discretizing the fourth-order eigenvalue problems using H^2-conforming finite element, a secant-type method was employed to compute the roots of the nonlinear function. Our method here is based on the ideas in [26, 27]. We first discretize (5) by the finite element method, we then apply a quadratic Jacobi-Davidson method with nonequivalence deflation to compute the eigenvalues of the resulting QEP. Contrary to the result in [19], our method is able to locate a large number of positive transmission eigenvalues of (5). Also, in [19], the authors only studied the isotropic case having the same Lamé coefficients and different densities, i.e., $(\lambda_0, \mu_0) = (\lambda_1, \mu_1)$, $\rho_0 \neq \rho_1$. In our paper, we consider the anisotropic elasticity with $\mathbf{C}_0 = \mathbf{C}_1, \rho_0 \neq \rho_1$ or $\mathbf{C}_0 \neq \mathbf{C}_1, \rho_0 = \rho_1$. The latter case is more practical representing the background and the perturbed bodies have different elastic behaviors.

Before ending the introduction, we would like to summarize the main contributions of this paper.

(i) We study the interior transmission eigenvalues problems for the elastic waves in which either $\rho_0 \neq \rho_1$ or $\mathbf{C}_0 \neq \mathbf{C}_1$. For these two cases, we reduce the PDE problems to GEPs by FEM. Due to the existence of non-physical zeros or infinities, in order to efficiently compute several hundred positive eigenvalues, GEPs are transformed to QEPs. The reduction of GEP to QEP in the first case was derived before. We then implement a quadratic Jacobi-Davidson algorithm to locate 500 positive eigenvalues of the QEP in the first case.

(ii) The second case where the elasticity tensors are different has never been studied numerically before. By mimicking the method for the first case, we try to convert the associated GEP to a QEP. Unfortunately, the naive attempt meets a special challenge in which a crucial matrix is degenerate in the second case. Consequently, a straightforward generalization of the transformations used for the first case fails in the second case. Here we discover a trick to circumvent this difficulty and derive a QEP that can be solved by the quadratic Jacobi-Davidson algorithm suitably combining with partial locking and partial deflation.

(iii) We are also interested in the behaviors of interior transmission eigenfunctions for the elastic waves. For the classical acoustic wave scattering, it was proved theoretically in [4] and demonstrated numerically in [3] that the interior transmission eigenfunction vanishes near the corner with the interior angle less than π and is localized near the corner with the interior angle greater than π. Our numerical results for the first case indicate the similar behaviors for the interior transmission eigenfunction. We want to point out that the ITEP for the elastic waves with only density jump is analogous to the acoustic wave scattering considered in [4] and [3]. Having the support of this numerical evidence, it is a natural question to verify the phenomenon rigorously.

(iv) For the second case, the behaviors of the interior transmission eigenfunctions near the boundary have never been investigated either theoretically or numerically. Intuitively, since the jump occurs in the leading order (i.e., in the elasticity tensor), one should study the behaviors of $\nabla\mathbf{u}$ and $\nabla\mathbf{v}$ near the boundary rather than $\mathbf{u}$ and $\mathbf{v}$. Our numerical simulations demonstrate that $\nabla\mathbf{u}$ and $\nabla\mathbf{v}$ are localized near the point where the interior angle is larger than π. We believe that proving this phenomenon rigorously is a daunting task.

(v) The resulting matrices derived from FEM are sparse and have large sizes. To be able to compute eigenvalues effectively, it is crucial to maintain sparsity in all matrix computations. Especially, in the second case, we have to deal with a *logically sparse* matrix given as the sum of a sparse matrix and a low-rank perturbation. The inverse of such matrix must be computed carefully using the Shermann-Morrison-Woodbury formula.

The paper is organized as follows. In Section 2, we introduce a GEP by discretizing the ITEP by FEM. In two cases considered in the paper, GEPs contain huge number of nonphysical eigenvalues. We then convert GEPs to QEPs in Section 3. Efficient quadratic Jacobi-Davidson method is discussed in Section 4. Numerical results are presented in Section 5. We end the paper with some conclusions and discussions in Section 6.

2 Discretization of ITEP

We first review the discretization of the ITEP (5) based on the standard piecewise linear FEM (see [15] for details). Let

$$\begin{aligned} S_h &= \text{The space of continuous piecewise linear functions on } D, \\ S_h^I &= \text{The subspace of functions in } S_h \text{ that have vanishing DoF on } \partial D, \\ S_h^B &= \text{The subspace of functions in } S_h \text{ that have vanishing DoF in } D, \end{aligned}$$

where DoF is the degrees of freedom. Let $\{\Phi_i\}_{i=1}^n$ and $\{\Psi_i\}_{i=1}^m$ denote standard nodal bases for the finite element spaces of S_h^I and S_h^B, respectively, then

$$\begin{aligned} \mathbf{u} = \mathbf{u}_h^I + \mathbf{u}_h^B &= \sum_{j=1}^n u_j \Phi_j + \sum_{j=1}^m w_j \Psi_j, \\ \mathbf{v} = \mathbf{v}_h^I + \mathbf{u}_h^B &= \sum_{j=1}^n v_j \Phi_j + \sum_{j=1}^m w_j \Psi_j. \end{aligned}$$

The choice of $\mathbf{u}_h^B$ in $\mathbf{v}$ is to ensure that (5c) is satisfied. Applying the standard piecewise linear finite element method to (5a) and using the integration by parts, we obtain

$$\begin{aligned} &\sum_{j=1}^n u_j (\sigma_{\mathbf{C}_0}(\Phi_j), \nabla \Phi_i) + \sum_{j=1}^m w_j (\sigma_{\mathbf{C}_0}(\Psi_j), \nabla \Phi_i) \\ &= \omega^2 \left(\sum_{j=1}^n u_j (\rho_0 \Phi_j, \Phi_i) + \sum_{j=1}^m w_j (\rho_0 \Psi_j, \Phi_i) \right). \end{aligned} \tag{6}$$

Matrix	Dimension	Definition
$K_l \succ 0,\ l=0,1,$	$n \times n$	interior space stiffness matrices: $(K_l)_{ij} = (\sigma_{\mathbf{C}_l}(\Phi_j), \nabla\Phi_i)$
$E_l,\ l=0,1,$	$n \times m$	interior/boundary stiffness matrices: $(E_l)_{ij} = (\sigma_{\mathbf{C}_l}(\Psi_j), \nabla\Phi_i)$
$M_l \succ 0,\ l=0,1,$	$n \times n$	interior space mass matrices: $(M_l)_{ij} = (\rho_l\Phi_j, \Phi_i)$
$F_l,\ l=0,1,$	$n \times m$	interior/boundary mass matrices: $(F_l)_{ij} = (\rho_l\Psi_j, \Phi_i)$
$G_l \succ 0,\ l=0,1,$	$m \times m$	boundary space stiffness matrices: $(G_l)_{ij} = (\sigma_{\mathbf{C}_l}(\Psi_j), \nabla\Psi_i)$
$H_l \succ 0,\ l=0,1,$	$m \times m$	boundary space mass matrices: $(H_l)_{ij} = (\rho_l\Psi_j, \Psi_i)$

Table 1: Stiffness and mass matrices for (6), (7), and (8).

Similarly, applying the standard piecewise linear finite element method to (5b), we have

$$\begin{aligned}&\sum_{j=1}^{n} v_j\left(\sigma_{\mathbf{C}_1}(\Phi_j), \nabla\Phi_i\right) + \sum_{j=1}^{m} w_j\left(\sigma_{\mathbf{C}_1}(\Psi_j), \nabla\Phi_i\right)\\ =&\omega^2\left(\sum_{j=1}^{n} v_j\left(\rho_1\Phi_j, \Phi_i\right) + \sum_{j=1}^{m} w_j\left(\rho_1\Psi_j, \Phi_i\right)\right).\end{aligned} \tag{7}$$

Remind that

$$(\sigma_{\mathbf{C}}(\Phi_j), \nabla\Phi_i) = \int_D \mathbf{C}\varepsilon(\Phi_j) : \varepsilon(\Phi_i)dx$$

and for the isotropic elasticity

$$(\sigma_{\mathbf{C}}(\Phi_j), \nabla\Phi_i) = \int_D \left\{2\mu\varepsilon(\Phi_j) : \varepsilon(\Phi_i) + \lambda(\nabla\cdot\Phi_j)\cdot(\nabla\cdot\Phi_i)\right\}dx,$$

where for matrices A and B, $A : B = \sum_{i,j} a_{ij}b_{ij}$. Finally, taking into account of (5c), (5d), applying the linear finite element method to the difference equation between (5a), (5b) and performing the integration by parts, yields

$$\begin{aligned}&\sum_{j=1}^{n}\left(u_j(\sigma_{\mathbf{C}_0}(\Phi_j), \nabla\Psi_i) - v_j(\sigma_{\mathbf{C}_1}(\Phi_j), \nabla\Psi_i)\right) + \sum_{j=1}^{m} w_j(\sigma_{\mathbf{C}_0}(\Psi_j) - \sigma_{\mathbf{C}_1}(\Psi_j), \nabla\Psi_i)\\ =\ &\omega^2\left(\sum_{j=1}^{n}\left(u_j(\rho_0\Phi_j, \Psi_i) - v_j(\rho_1\Phi_j, \Psi_i)\right) + \sum_{j=1}^{m} w_j((\rho_0-\rho_1)\Psi_j, \Psi_i)\right).\end{aligned} \tag{8}$$

Hereafter, we define the stiffness matrices K_l, E_l, G_l, and mass matrices M_l, F_l, H_l as in Table 1. In addition, we set $\mathbf{u} = [u_1, \ldots, u_n]^\top$, $\mathbf{v} = [v_1, \ldots, v_n]^\top$, and $\mathbf{w} = [w_1, \ldots, w_m]^\top$. Then, the discretizations of (6), (7) and (8) give rise to a generalized eigenvalue problem (GEP)

$$\mathcal{A}\mathbf{z} = \lambda \mathcal{B}\mathbf{z} \tag{9a}$$

with $\lambda = \omega^2$,

$$\mathcal{A} = \begin{bmatrix} K_0 & 0 & E_0 \\ 0 & K_1 & E_1 \\ E_0^\top & -E_1^\top & G_0 - G_1 \end{bmatrix}, \ \mathcal{B} = \begin{bmatrix} M_0 & 0 & F_0 \\ 0 & M_1 & F_1 \\ F_0^\top & -F_1^\top & H_0 - H_1 \end{bmatrix}, \ \mathbf{z} = \begin{bmatrix} \mathbf{u} \\ \mathbf{v} \\ \mathbf{w} \end{bmatrix}. \tag{9b}$$

3 GEP to QEP

Our next aim is to convert the GEP (9) into a quadratic eigenvalue problem (QEP). We now discuss two cases separately.

Case 1. For this, we assume that $\mathbf{C}_0 = \mathbf{C}_1$ and $\rho_0 > \rho_1$. Thus, we have $K_0 = K_1 = K, E_0 = E_1 = E, G_0 = G_1$. This is exactly the same system considered in [26]. The difficulty of locating a bunch of eigenvalues near the left most of the positive axis lies in the fact that there are too many zero eigenvalues. To see this, we compute the null space of $\mathcal{A}$. It is clear that $\mathcal{A}\mathbf{z} = 0$ is equivalent to

$$\begin{cases} K\mathbf{u} + E\mathbf{w} = 0 \Leftrightarrow \mathbf{u} = -K^{-1}E\mathbf{w}, \\ K\mathbf{v} + E\mathbf{w} = 0 \Leftrightarrow \mathbf{v} = -K^{-1}E\mathbf{w}, \\ E^\top \mathbf{u} - E^\top \mathbf{v} = 0. \end{cases} \tag{10}$$

Therefore, for any $\mathbf{w} \neq 0$, $(-K^{-1}E\mathbf{w}, -K^{-1}E\mathbf{w}, \mathbf{w})$ belongs to $\mathrm{null}(\mathcal{A})$. In other words, $\dim(\mathrm{null}(\mathcal{A})) = m$. Since we have a cluster of zero eigenvalues, the usual GEP solver is ineffective in finding the positive eigenvalues we are interested. So we follow the ideas in [26] (precisely in [18]) converting the GEP to the QEP. We now write

$$\begin{aligned} &H = H_0 - H_1, \quad M = M_0 - M_1, \quad F = F_0 - F_1, \\ &\widehat{M}_1 = M_1 - F_1 H^{-1} F^\top, \quad \widehat{M} = M - FH^{-1}F^\top, \quad \widehat{K} = K - EH^{-1}F^\top, \end{aligned}$$

and

$$\mathcal{S} = \begin{bmatrix} K & E \end{bmatrix}, \quad \mathcal{T}_1 = \begin{bmatrix} M_1 & F_1 \end{bmatrix}, \quad \mathcal{M} = \begin{bmatrix} M & F \\ F^\top & H \end{bmatrix}.$$

Since $\rho_0 > \rho_1$, we can see that $H \succ 0$, $M \succ 0$, and $\mathcal{M} \succ 0$. We also have $\widehat{M} \succ 0$. The λ-matrix $\mathcal{L}(\lambda)$ in (9) is now written as

$$\mathcal{L}(\lambda) = \begin{bmatrix} K - \lambda(M + M_1) & 0 & E - \lambda(F + F_1) \\ 0 & K - \lambda M_1 & E - \lambda F_1 \\ E^\top - \lambda(F^\top + F_1^\top) & -E^\top + \lambda F_1^\top & -\lambda H \end{bmatrix}. \tag{11}$$

Introducing two invertible matrices

$$\mathcal{J} = \begin{bmatrix} I_n & 0 & 0 \\ 0 & -I_n & 0 \\ 0 & 0 & I_n \end{bmatrix}, \quad \mathcal{P} = \begin{bmatrix} 0 & I_n & 0 \\ -I_n & I_n & 0 \\ 0 & 0 & I_n \end{bmatrix}.$$

We can transform $\mathcal{L}(\lambda)$ to a symmetric λ-matrix

$$\mathcal{J}\mathcal{P}\mathcal{L}(\lambda)\mathcal{P} = \begin{bmatrix} -K + \lambda M_1 & K - \lambda M_1 & E - \lambda F_1 \\ K - \lambda M_1 & -\lambda M & -\lambda F \\ E^\top - \lambda F_1^\top & -\lambda F^\top & -\lambda H \end{bmatrix} = \begin{bmatrix} -K + \lambda M_1 & \mathcal{S} - \lambda \mathcal{T}_1 \\ (\mathcal{S} - \lambda \mathcal{T}_1)^\top & -\lambda \mathcal{M} \end{bmatrix}.$$

Furthermore, let

$$\mathcal{C}(\lambda) = \begin{bmatrix} I_n & 0 \\ \lambda^{-1}\mathcal{M}^{-1}(\mathcal{S} - \lambda \mathcal{T}_1)^\top & I_{n+m} \end{bmatrix}$$

then we can compute

$$\begin{aligned} &(\mathcal{C}(\lambda))^\top (\mathcal{J}\mathcal{P}\mathcal{L}(\lambda)\mathcal{P})\mathcal{C}(\lambda) \\ &= \begin{bmatrix} -K + \lambda M_1 + \lambda^{-1}(\mathcal{S} - \lambda \mathcal{T}_1)\mathcal{M}^{-1}(\mathcal{S} - \lambda \mathcal{T}_1)^\top & 0 \\ 0 & -\lambda \mathcal{M} \end{bmatrix} \\ &= \begin{bmatrix} \lambda^{-1}\mathcal{Q}(\lambda) & 0 \\ 0 & -\lambda \mathcal{M} \end{bmatrix}, \end{aligned}$$

where

$$\mathcal{Q}(\lambda) \equiv \left(\lambda^2 A_2 + \lambda A_1 + A_0\right), \tag{12}$$

with $A_2,\ A_1$ and A_0 being $n \times n$ symmetric matrices given by

$$\begin{aligned} A_2 &= M_1 + \widehat{M}_1 \widehat{M}^{-1} \widehat{M}_1^\top + F_1 H^{-1} F_1^\top && \text{(13a)} \\ &= M_1 + \mathcal{T}_1 \mathcal{M}^{-1} \mathcal{T}_1^\top, \\ A_1 &= -K - \widehat{K}\widehat{M}^{-1}\widehat{M}_1^\top - \widehat{M}_1 \widehat{M}^{-1} \widehat{K}^\top - E H^{-1} F_1^\top - F_1 H^{-1} E^\top && \text{(13b)} \\ &= -K - \mathcal{S}\mathcal{M}^{-1}\mathcal{T}_1^\top - \mathcal{T}_1 \mathcal{M}^{-1} \mathcal{S}^\top, \\ A_0 &= \widehat{K}\widehat{M}^{-1}\widehat{K}^\top + E H^{-1} E^\top && \text{(13c)} \\ &= \mathcal{S}\mathcal{M}^{-1}\mathcal{S}^\top. \end{aligned}$$

It has been shown [18] that the GEP (9) can be reduced to the QEP as in (12) and (13) in which all nonphysical zero are removed.

Theorem 1. [18] *Let $\mathcal{L}(\lambda)$ and $\mathcal{Q}(\lambda)$ be defined as in* (9) *and* (12)*, respectively. Then*

$$\sigma(\mathcal{L}(\lambda)) = \underbrace{\{0, \cdots, 0\}}_{m} \cup \sigma(\mathcal{Q}(\lambda)).$$

Here, $\sigma(\cdot)$ denotes the spectrum of the associated matrix pencil.

Case 2. Now we assume $\rho_0 = \rho_1$ and $\mathbf{C}_0 > \mathbf{C}_1$ in the sense of (2). Then $M_0 = M_1 = M$, $F_0 = F_1 = F$, $H_0 - H_1 = 0$, and (9) becomes

$$\mathcal{A}\mathbf{z} = \lambda\mathcal{B}\mathbf{z} \tag{14}$$

with

$$\mathcal{A} = \begin{bmatrix} K_0 & 0 & E_0 \\ 0 & K_1 & E_1 \\ E_0^\top & -E_1^\top & G_0 - G_1 \end{bmatrix}, \ \mathcal{B} = \begin{bmatrix} M & 0 & F \\ 0 & M & F \\ F^\top & -F^\top & 0 \end{bmatrix}. \tag{15}$$

Similar to the observation (10), we can see that $\mathrm{null}(\mathcal{B}) = m$. Consequently, the GEP (14) has m infinite eigenvalues. Since we are interested in locating eigenvalues in the leftmost positive axis, those m infinite eigenvalues seems harmless. It looks like one may try to solve the GEP (14) directly. However, even here GEP is not ineffective due to the excessive number of complex eigenvalues. So we will again convert the GEP (14) to a QEP.

Changing λ to λ^{-1}, (14) is equivalent to

$$\mathcal{B}\mathbf{z} = \lambda\mathcal{A}\mathbf{z}. \tag{16}$$

In other words, we are interested in locating eigenvalues of (16) in the rightmost positive axis. Now (16) has m nonphysical zeros. Like in **Case 1**, defining $K = K_0 - K_1$, $E = E_0 - E_1$, and $G = G_0 - G_1$, the corresponding λ-matrix $\widetilde{\mathcal{L}}(\lambda)$ of (16) becomes

$$\widetilde{\mathcal{L}}(\lambda) = \begin{bmatrix} M - \lambda(K + K_1) & 0 & F - \lambda(E + E_1) \\ 0 & M - \lambda K_1 & F - \lambda E_1 \\ F^\top - \lambda(E + E_1)^\top & -F^\top + \lambda E_1^\top & -\lambda G \end{bmatrix}, \tag{17}$$

which is nothing but (11). Therefore, as in **Case 1**, we can transform $\widetilde{\mathcal{L}}(\lambda)$ to a symmetric λ-matrix

$$\mathcal{J}\mathcal{P}\widetilde{\mathcal{L}}(\lambda)\mathcal{P} = \begin{bmatrix} -M + \lambda K_1 & M - \lambda K_1 & F - \lambda E_1 \\ M - \lambda K_1 & -\lambda K & -\lambda E \\ F^\top - \lambda E_1^\top & -\lambda E^\top & -\lambda G \end{bmatrix} = \begin{bmatrix} -M + \lambda K_1 & \mathcal{R} - \lambda\mathcal{U}_1 \\ (\mathcal{R} - \lambda\mathcal{U}_1)^\top & -\lambda\mathcal{K} \end{bmatrix},$$

where

$$\mathcal{R} = \begin{bmatrix} M & F \end{bmatrix}, \quad \mathcal{U}_1 = \begin{bmatrix} K_1 & E_1 \end{bmatrix}, \quad \mathcal{K} = \begin{bmatrix} K & E \\ E^\top & G \end{bmatrix}.$$

Likewise, since $\mathbf{C}_0 > \mathbf{C}_1$, we can see that $G \succ 0$, $K \succ 0$. However, in this case, the matrix $\mathcal{K}$ may be degenerate. We can not proceed what we did in **Case 1**. To further analyze this case, we assume that

$$\mathrm{null}\,(\mathcal{K}) = \mathrm{span}\{\mathbf{v}_1, \cdots, \mathbf{v}_k\}$$

and denote $V_0 = [\mathbf{v}_1, \cdots, \mathbf{v}_k] \in \mathbb{R}^{(n+m)\times k}$. Then there exist a series of Householder transforms

$$Q = (I - 2\frac{\mathbf{q}_k\mathbf{q}_k^\top}{\mathbf{q}_k^\top\mathbf{q}_k}) \cdot \cdots \cdot (I - 2\frac{\mathbf{q}_1\mathbf{q}_1^\top}{\mathbf{q}_1^\top\mathbf{q}_1})$$

such that

$$QV_0 = \begin{bmatrix} 0 \\ \Gamma \end{bmatrix},$$

where Γ is a $k \times k$ nonsingular triangular matrix. Note that Q is orthogonal and can be written as

$$Q = I - WY^\top \tag{18}$$

with $W, Y \in \mathbb{R}^{(n+m)\times k}$.

It is not hard to check that

$$Q\mathcal{K}Q^\top = \begin{bmatrix} \widehat{\mathcal{K}} & 0 \\ 0 & 0 \end{bmatrix},$$

where

$$\begin{aligned} \widehat{\mathcal{K}} &= \begin{bmatrix} I_{(n+m)-k} & 0 \end{bmatrix} (\mathcal{K} - \mathcal{K}YW^\top - WY^\top\mathcal{K} + W(Y^\top\mathcal{K}Y)W^\top) \begin{bmatrix} I_{(n+m)-k} \\ 0 \end{bmatrix} \\ &= \mathcal{K}_1 + \begin{bmatrix} \widetilde{Y} & \widetilde{W} \end{bmatrix} \begin{bmatrix} 0 & -I_k \\ -I_k & \widetilde{\mathcal{K}} \end{bmatrix} \begin{bmatrix} \widetilde{Y}^\top \\ \widetilde{W}^\top \end{bmatrix} \end{aligned} \tag{19}$$

and

$$\mathcal{K}_1 = \begin{bmatrix} I_{(n+m)-k} & 0 \end{bmatrix} \mathcal{K} \begin{bmatrix} I_{(n+m)-k} \\ 0 \end{bmatrix}, \quad \widetilde{\mathcal{K}} = Y^\top\mathcal{K}Y,$$

$$\widetilde{Y} = \begin{bmatrix} I_{(n+m)k} & 0 \end{bmatrix} \mathcal{K}Y, \quad \widetilde{W} = \begin{bmatrix} I_{(n+m)-k} & 0 \end{bmatrix} W.$$

Note that $\mathcal{K}_1$ is invertible. It is important to point out that since $\mathcal{K}$ is sparse and so is $\mathcal{K}_1$. We observe from (19) that $\widehat{\mathcal{K}}$ is written as the sum of a sparse matrix and a low-rank perturbation. For that, $\widehat{\mathcal{K}}$ is called *logically sparse*. This property is crucial in order to compute $\widehat{\mathcal{K}}^{-1}$ efficiently. More precisely, in view of (19), $\widehat{\mathcal{K}}^{-1}$ can be obtained efficiently by using the Shermann-Morrison-Woodbury formula.

We now write

$$\begin{bmatrix} I_n & 0 \\ 0 & Q \end{bmatrix} \begin{bmatrix} -M + \lambda K_1 & \mathcal{R} - \lambda\mathcal{U}_1 \\ (\mathcal{R} - \lambda\mathcal{U}_1)^\top & -\lambda\mathcal{K} \end{bmatrix} \begin{bmatrix} I_n & 0 \\ 0 & Q^\top \end{bmatrix} = \begin{bmatrix} -M + \lambda K_1 & \widehat{\mathcal{R}} - \lambda\widehat{\mathcal{U}}_1 & (S - \lambda T) \\ (\widehat{\mathcal{R}} - \lambda\widehat{\mathcal{U}}_1)^\top & -\lambda\widehat{\mathcal{K}} & 0 \\ (S - \lambda T)^\top & 0 & 0 \end{bmatrix},$$

where

$$\begin{bmatrix} \widehat{\mathcal{R}} - \lambda\widehat{\mathcal{U}}_1 & (S - \lambda T) \end{bmatrix} = (\mathcal{R} - \lambda\mathcal{U}_1)Q^\top. \tag{20}$$

Thus GEP (16) is equivalent to

$$\begin{bmatrix} -M + \lambda K_1 & \widehat{\mathcal{R}} - \lambda\widehat{\mathcal{U}}_1 & (S - \lambda T) \\ (\widehat{\mathcal{R}} - \lambda\widehat{\mathcal{U}}_1)^\top & -\lambda\widehat{\mathcal{K}} & 0 \\ (S - \lambda T)^\top & 0 & 0 \end{bmatrix} \begin{bmatrix} \mathbf{x} \\ \mathbf{y} \\ \mathbf{z} \end{bmatrix} = 0,$$

namely,

$$(-M+\lambda K_1)\mathbf{x}+(\widehat{\mathcal{R}}-\lambda\widehat{\mathcal{U}}_1)\mathbf{y}+(S-\lambda T)\mathbf{z}=0, \tag{21a}$$

$$(\widehat{\mathcal{R}}-\lambda\widehat{\mathcal{U}}_1)^\top\mathbf{x}-\lambda\widehat{\mathcal{K}}\mathbf{y}=0, \tag{21b}$$

$$(S-\lambda T)^\top\mathbf{x}=0. \tag{21c}$$

It follows from (21b) that

$$\mathbf{y}=\frac{1}{\lambda}\widehat{\mathcal{K}}^{-1}(\widehat{\mathcal{R}}-\lambda\widehat{\mathcal{U}}_1)^\top\mathbf{x}.$$

Substituting this relation into (21a) and combining (21c) gives

$$\left(\lambda\begin{bmatrix}-M & S\\ S^\top & 0\end{bmatrix}+\lambda^2\begin{bmatrix}K_1 & -T\\ -T^\top & 0\end{bmatrix}+\begin{bmatrix}\widehat{\mathcal{R}}\widehat{\mathcal{K}}^{-1}\widehat{\mathcal{R}}^\top & 0\\ 0 & 0\end{bmatrix}-\lambda\begin{bmatrix}\widehat{\mathcal{U}}_1\widehat{\mathcal{K}}^{-1}\widehat{\mathcal{R}}^\top+\widehat{\mathcal{R}}\widehat{\mathcal{K}}^{-1}\widehat{\mathcal{U}}_1^\top & 0\\ 0 & 0\end{bmatrix}\right.$$
$$\left.+\lambda^2\begin{bmatrix}\widehat{\mathcal{U}}_1\widehat{\mathcal{K}}^{-1}\widehat{\mathcal{U}}_1^\top & 0\\ 0 & 0\end{bmatrix}\right)\begin{bmatrix}\mathbf{x}\\ \mathbf{z}\end{bmatrix}=0,$$

that is,

$$\begin{aligned}&\left(\lambda^2\begin{bmatrix}K_1+\widehat{\mathcal{U}}_1\widehat{\mathcal{K}}^{-1}\widehat{\mathcal{U}}_1^\top & -T\\ -T^\top & 0\end{bmatrix}+\lambda\begin{bmatrix}-M-\widehat{\mathcal{U}}_1\widehat{\mathcal{K}}^{-1}\widehat{\mathcal{R}}^\top-\widehat{\mathcal{R}}\widehat{\mathcal{K}}^{-1}\widehat{\mathcal{U}}_1^\top & S\\ S^\top & 0\end{bmatrix}\right.\\ &\left.+\begin{bmatrix}\widehat{\mathcal{R}}\widehat{\mathcal{K}}^{-1}\widehat{\mathcal{R}}^\top & 0\\ 0 & 0\end{bmatrix}\right)\begin{bmatrix}\mathbf{x}\\ \mathbf{z}\end{bmatrix}=0.\end{aligned} \tag{22}$$

As in Theorem 1, m zero eigenvalues of GEP (16) have been removed from the QEP (22). It is helpful to remind that (22) is derived with the aim of finding eigenvalues in the rightmost positive axis. However, we are interested in locating eigenvalues in the leftmost positive axis. So we modify (22) into

$$\begin{aligned}&\left(\lambda^2\begin{bmatrix}\widehat{\mathcal{R}}\widehat{\mathcal{K}}^{-1}\widehat{\mathcal{R}}^\top & 0\\ 0 & 0\end{bmatrix}+\lambda\begin{bmatrix}-M-\widehat{\mathcal{U}}_1\widehat{\mathcal{K}}^{-1}\widehat{\mathcal{R}}^\top-\widehat{\mathcal{R}}\widehat{\mathcal{K}}^{-1}\widehat{\mathcal{U}}_1^\top & S\\ S^\top & 0\end{bmatrix}\right.\\ &\left.+\begin{bmatrix}K_1+\widehat{\mathcal{U}}_1\widehat{\mathcal{K}}^{-1}\widehat{\mathcal{U}}_1^\top & -T\\ -T^\top & 0\end{bmatrix}\right)\begin{bmatrix}\mathbf{x}\\ \mathbf{z}\end{bmatrix}=0.\end{aligned} \tag{23}$$

QEP (23) now can be solved by the Jacobi-Davidson method.

4 Efficient quadratic Jacobi-Davidson algorithm

After transforming the GEP to the QEP, our goal now is to find positive eigenvalues of

$$\mathcal{Q}(\lambda)=\lambda^2A_2+\lambda A_1+A_0,$$

with A_2, A_1, A_0 being given in (13) in **Case 1** and

$$A_2=\begin{bmatrix}\widehat{\mathcal{R}}\widehat{\mathcal{K}}^{-1}\widehat{\mathcal{R}}^\top & 0\\ 0 & 0\end{bmatrix},\quad A_1=\begin{bmatrix}-M-\widehat{\mathcal{U}}_1\widehat{\mathcal{K}}^{-1}\widehat{\mathcal{R}}^\top-\widehat{\mathcal{R}}\widehat{\mathcal{K}}^{-1}\widehat{\mathcal{U}}_1^\top & S\\ S^\top & 0\end{bmatrix}$$
$$A_0=\begin{bmatrix}K_1+\widehat{\mathcal{U}}_1\widehat{\mathcal{K}}^{-1}\widehat{\mathcal{U}}_1^\top & -T\\ -T^\top & 0\end{bmatrix}$$

in **Case 2**. For **Case 1**, the quadratic polynomial $\mathcal{Q}(\lambda)$ is similar to that in [26, 27]. So the Jacobi-Davidson algorithm combining with a partial locking scheme developed there can be applied to $\mathcal{Q}(\lambda)$ to locate eigenvalues in the leftmost positive axis.

We will pay more attention to **Case 2** since $\mathcal{Q}(\lambda)$ is obtained by modifying sparse matrices with appropriate Householder transforms Q. It is important to maintain the sparsity of matrices for computational efficiency. At each step of the Jacobi-Davidson algorithm for QEP (23), we have to solve the linear system (with a shift θ) of the correction equation

$$\mathcal{Q}(\theta)\mathbf{t} := \begin{bmatrix} K_1 - \theta M + (\widehat{\mathcal{U}}_1 - \theta\widehat{\mathcal{R}})\widehat{\mathcal{K}}^{-1}(\widehat{\mathcal{U}}_1 - \theta\widehat{\mathcal{R}})^\top & \theta S - T \\ (\theta S - T)^\top & 0 \end{bmatrix} \begin{bmatrix} \mathbf{t}_1 \\ \mathbf{t}_3 \end{bmatrix} = \begin{bmatrix} \mathbf{b}_1 \\ \mathbf{b}_3 \end{bmatrix}. \tag{24}$$

For the sake of computational efficiency, it is not advisable to solve (24) directly. Here is a trick. Observe that (24) is equivalent to

$$\begin{bmatrix} K_1 - \theta M & \widehat{\mathcal{U}}_1 - \theta\widehat{\mathcal{R}} & (\theta S - T) \\ (\widehat{\mathcal{U}}_1 - \theta\widehat{\mathcal{R}})^\top & -\widehat{\mathcal{K}} & 0 \\ (\theta S - T)^\top & 0 & 0 \end{bmatrix} \begin{bmatrix} \mathbf{t}_1 \\ \mathbf{t}_2 \\ \mathbf{t}_3 \end{bmatrix} = \begin{bmatrix} \mathbf{b}_1 \\ 0 \\ \mathbf{b}_3 \end{bmatrix},$$

with $\mathbf{t}_2 = \widehat{\mathcal{K}}^{-1}(\theta\widehat{\mathcal{R}} - \widehat{\mathcal{U}}_1)^\top \mathbf{t}_1$; that is

$$\begin{bmatrix} K_1 - \theta M & \mathcal{U}_1 - \theta\mathcal{R} \\ (\mathcal{U}_1 - \theta\mathcal{R})^\top & -\mathcal{K} \end{bmatrix} \begin{bmatrix} \mathbf{t}_1 \\ \tilde{\mathbf{t}}_2 \end{bmatrix} = \begin{bmatrix} \mathbf{b}_1 \\ \tilde{\mathbf{b}}_2 \end{bmatrix}, \tag{25}$$

where

$$\tilde{\mathbf{t}}_2 = Q^\top \begin{bmatrix} \mathbf{t}_2 \\ \mathbf{t}_3 \end{bmatrix}, \quad \tilde{\mathbf{b}}_2 = Q^\top \begin{bmatrix} 0 \\ \mathbf{b}_3 \end{bmatrix}. \tag{26}$$

Now once $\begin{bmatrix} \mathbf{t}_1 \\ \tilde{\mathbf{t}}_2 \end{bmatrix}$ of (25) is solved with MATLAB in sparse version, we can find the solution $\begin{bmatrix} \mathbf{t}_1 \\ \mathbf{t}_3 \end{bmatrix}$ for (24) using the first formula of (26). Note that

$$\begin{bmatrix} \mathbf{t}_2 \\ \mathbf{t}_3 \end{bmatrix} = Q\tilde{\mathbf{t}}_2 = (I - WY^\top)\tilde{\mathbf{t}}_2 = \tilde{\mathbf{t}}_2 - WY^\top\tilde{\mathbf{t}}_2.$$

Therefore, we only need to multiply $\tilde{\mathbf{t}}_2$ by a lower rank matrix to obtain $\mathbf{t}_3$.

Let the matrix V_k have been selected in the Jacobi-Davidson algorithm. We then define

$$\mathcal{Q}_k(\lambda) = \lambda^2 V_k A_2 V_k + \lambda V_k A_1 V_k + V_k A_0 V_k := \lambda^2 A_2^{(k)} + \lambda A_1^{(k)} + A_0^{(k)}.$$

Select a suitable eigenpair $(\hat{\theta}, \hat{\mathbf{s}})$ with $\mathcal{Q}_k(\hat{\theta})\hat{\mathbf{s}} = 0$ and $\|\hat{\mathbf{s}}\|_2 = 1$. We now compute

$$\mathbf{u}_k = V_k\hat{\mathbf{s}}, \quad \mathbf{r}_k = \mathcal{Q}(\hat{\theta})\mathbf{u}_k, \quad \mathbf{p}_k = \mathcal{Q}'(\hat{\theta})\mathbf{u}_k$$

and solve the correction equation for the search direction $\mathbf{t}$:

$$(I - \frac{\mathbf{p}_k \mathbf{u}_k^\top}{\mathbf{u}_k^\top \mathbf{p}_k}) \mathcal{Q}(\hat{\theta})(I - \mathbf{u}_k \mathbf{u}_k^\top)\mathbf{t} = -\mathbf{r}_k \quad \text{with} \quad \mathbf{t} \perp \mathbf{u}_k. \tag{27}$$

It turns out the solution of (27) can be obtained by computing

$$\mathbf{t}_k = -\mathcal{Q}(\hat{\theta})^{-1}\mathbf{r}_k + \eta_k \mathcal{Q}(\hat{\theta})^{-1}\mathbf{p}_k \quad \text{and} \quad \eta_k = \frac{\mathbf{u}_k^\top \mathcal{Q}(\hat{\theta})^{-1}\mathbf{r}_k}{\mathbf{u}_k^\top \mathcal{Q}(\hat{\theta})^{-1}\mathbf{p}_k}. \tag{28}$$

In (28), vectors $\mathcal{Q}(\hat{\theta})^{-1}\mathbf{r}_k, \mathcal{Q}(\hat{\theta})^{-1}\mathbf{p}_k$ can be computed by solving the linear system (24) via (25) and (26) efficiently.

We now use the solution $\mathbf{t}_k$ of the correction equation (27) to expand the matrix V_k. Let

$$\tilde{\mathbf{v}}_{k+1} = \mathbf{t}_k - (\mathbf{t}_k^\top V_k)V_k \quad \text{and} \quad \mathbf{v}_{k+1} = \frac{\tilde{\mathbf{v}}_{k+1}}{\|\tilde{\mathbf{v}}_{k+1}\|_2},$$

then $\mathbf{v}_{k+1} \perp V_k$ and $\|\mathbf{v}_{k+1}\|_2 = 1$. Define $V_{k+1} = \begin{bmatrix} V_k & \mathbf{v}_{k+1} \end{bmatrix}$ and update

$$\mathcal{Q}_{k+1}(\lambda) = V_{k+1}^\top \mathcal{Q}(\lambda) V_{k+1} = \lambda^2 A_2^{(k+1)} + \lambda A_1^{(k+1)} + A_0^{(k+1)},$$

where $A_j^{(k+1)}, j = 0, 1, 2$, are symmetric matrices with the updated last columns computed by the following formulas, respectively,

$$\text{last column of } A_j^{(k+1)} = \begin{bmatrix} V_k^\top \\ \mathbf{v}_{k+1}^\top \end{bmatrix} A_j \mathbf{v}_{k+1}.$$

Finally, in order to compute a large number of positive eigenvalues successively, partial deflation and partial locking schemes are necessary. We refer the reader to [26] for detailed descriptions of the methods.

For sake of completeness, we briefly describe the partial deflation scheme. Let $Y_0 = A_0 X_1 \Lambda_1^{-1}$ and $Y_2 = A_2 X_1$ and define

$$\begin{aligned} \tilde{A}_2 &= A_2 - Y_2 \Theta_1 Y_2^\top \\ \tilde{A}_1 &= A_1 + Y_2 \Theta_1 Y_0^\top + Y_0 \Theta_1 Y_2^\top \\ \tilde{A}_0 &= A_0 - Y_0 \Theta_1 Y_0^\top \end{aligned}$$

with $\Theta_1 := (X_1^\top A_2 X_1)^{-1}$ for (Λ_1, X_1) being an eigenmatrix pair of $\mathcal{Q}(\lambda)$ of (23). Then the QEP after deflation is

$$\mathcal{Q}_d(\lambda)\mathbf{p} \equiv (\lambda^2 \tilde{A}_2 + \lambda \tilde{A}_1 + \tilde{A}_0)\mathbf{p} = 0.$$

Moreover, setting $U = \theta Y_2 - Y_0$, we can solve the correction equation efficiently by solving the linear system

$$\mathcal{Q}(\theta)\mathbf{Z} = \begin{bmatrix} \tilde{\mathbf{p}} & \tilde{\mathbf{r}} & U \end{bmatrix}.$$

where $\tilde{\mathbf{r}} = \mathcal{Q}_d(\theta)\tilde{\mathbf{u}}$ and $\tilde{\mathbf{p}} = (2\theta\tilde{A}_2 + \tilde{A}_1)\tilde{\mathbf{u}}$. We then define the correction vector $\mathbf{t}_d$ for the deflated QEP by

$$\mathbf{t}_d = \frac{\tilde{\mathbf{u}}^\top \tilde{\mathbf{t}}_2}{\tilde{\mathbf{u}}^\top \tilde{\mathbf{t}}_1}\tilde{\mathbf{t}}_1 - \tilde{\mathbf{t}}_2, \tag{29}$$

where

$$\begin{bmatrix}\tilde{\mathbf{t}}_1 & \tilde{\mathbf{t}}_2\end{bmatrix} = \mathbf{Z}(:,1:2) + \mathbf{Z}(:,3:r+2)(\Theta_1^{-1} - U^\top \mathbf{Z}(:,3:r+2))^{-1}U^\top \mathbf{Z}(:,1:2)$$

and $r = \operatorname{rank} V_1$.

The algorithms for our methods are given below.

Algorithm 1 Quadratic Jacobi-Davidson with partial locking for **Case 1**

Input: Coefficient Matrices A_0, A_1, A_2, locking number l and an initial orthonormal matrix V.

Output: The desired eigenpairs $(\lambda_j, \mathbf{x}_j)$ for $j = 1, \cdots, p$ and the desired eigenvector of GEP in **Case 1**.

```
Set V_c = [ ]
for j = 1, ..., p do
  while (the desired eigenpair is not convergent) do
    Compute the eigenpair (θ, s) of V* Q(θ) V s = 0 with ||s|| = 1;
    Solve the correction equation (see [26, 27]);
    Orthogonalize t against V; set V = [V, t/||t||];
  end while
  Set λ_j = θ and x_j = s;
  if j ≤ l then
    Orthogonalize x_j against V_c; set V_c = [V_c, x_j/||x_j||];
  else
    Orthogonalize x_j against V_c(:, 2 : l); set V_c = [V_c(:, 2 : l), x_j/||x_j||];
  end if
  Set V ≡ [V_c, V_0] with V_0^T V_0 = I;
end for
Evaluate x = λ_1^{-1} M^{-1} (S − T_1)^T x_1;
Set z = [x(1 : n); x(1 : n) − x_1; x(n + 1 : end)]
```

Algorithm 2 Quadratic Jacobi-Davidson with partial locking or partial deflation for **Case 2**

Input: Mass matrices M, F, stiffness matrices K_0, K_1, E_0, E_1, G and locking or deflation number l.

Output: The desired eigenpairs $(\lambda_j, \mathbf{x}_j)$, $j = 1, \cdots, p$ and the associated eigenvector for GEP in **Case 2**.

Set $\mathcal{K} = \begin{bmatrix} K & E \\ E^\top & G \end{bmatrix}$;
Compute $\mathcal{N}_\mathcal{K}$ by shift-and-invert Lanczos method; Set $N = \mathbf{rank}(\mathcal{N}_\mathcal{K})$;
for $i = 1, \cdots, N$ **do**
  Set $\mathbf{g} = \mathcal{N}_\mathcal{K}(1 : end - i + 1, i)$;
  Compute $\mathbf{q} = \mathbf{g} - \mathrm{sgn}(\mathbf{g}(end))\|\mathbf{g}\| e_{(n+m)-i+1}$; Set $W(1 : \mathrm{length}(\mathbf{q}), i) = \mathbf{q}$;
  Compute $\mathcal{N}_\mathcal{K}(1 : end - i + 1, i : end) = \mathcal{N}_\mathcal{K}(1 : end - i + 1, i : end) - 2\mathbf{q}\mathbf{q}^\top \mathcal{N}_\mathcal{K}(1 : end - i + 1, i : end)$;
end for
Compute $Q = \prod_{i=1}^{N} \left(I - 2\frac{W(:, i)W(:, i)^\top}{W(:, i)^\top W(:, i)} \right)$;
Compute additional matrices Y satisfying (18);
Compute the coefficient matrices A_0, A_1 and A_2 according to (23);
for $j = 1, \cdots, p$ **do**
  Apply Jacobi-Davidson with partial locking scheme or with partial deflation scheme based on the correction equation (25) or (29), respectively;
end for
Set $\mathcal{D} = \mathcal{A} - \lambda_1 \mathcal{B}$ defined in (15);
Compute the associated eigenvector $\mathbf{z}$ by shift-and-invert Lanczos on $\mathcal{D}$

5 Numerical results

In our numerical simulations, we consider seven domains. Standard triangular meshes with equal mesh length about 0.04 are generated for these domains. The number of interior points and of boundary points are denoted by a and b, respectively, and are shown in the table of meshes below. Since we are ealing with the elasticity system in the plane, the dimensions of stiffness and mass matrices in Table 1 are doubled, i.e., $n = 2a$ and $m = 2b$. All computations were carried out in Matlab. Additionally, the hardware configurations used were two servers equipped with Intel Quad-Core Xeon X5560 2.80GHz CPUs installing Matlab R2014a and Intel 12-Core Xeon E5-2697 2.70GHz CPUs installing Matlab R2017b and 58GB and 256GB of main memory, respectively.

Disc	Ellipse	Triangle	Cone
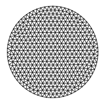	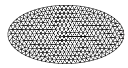	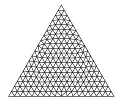	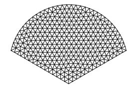
$(143841, 1270)$	$(71590, 970)$	$(79800, 1200)$	$(108203, 1235)$

Dumbbell	Square	Mouth
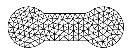	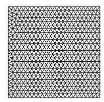	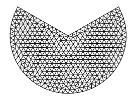
$(121829, 1556)$	$(140848, 1400)$	$(95885, 1221)$

Table 2: Meshes for different domains

We consider the isotropic elasticity (3) in the simulations. In our numerical results, we also show the values of eigenvector corresponding to the first positive eigenvalue for both **Case 1** and **Case 2**. The purpose of showing these results is to explore the behaviors of the interior transmission eigenfunctions near corners for the elastic waves. In the classical acoustic waves, it was proved theoretically in [4] and demonstrated numerically in [3] that the interior transmission eigenfunction vanishes near the corner with the interior angle less than π and is localized near the corner with the interior angle greater than π. Our numerical results indicate that a similar behavior occurs for the elastic waves.

Case 1. In the simulations, we choose $\mu_0 = \mu_1 = 5$, $\lambda_0 = \lambda_1 = 5$, $\rho_0 = 50$, $\rho_1 = 1$. We implement **Algorithm 1** to this case and locate first 500 positive eigenvalues (i.e., $p = 500$) and the associated eigenvector of the first positive eigenvalue. Results are shown in Figure 1.

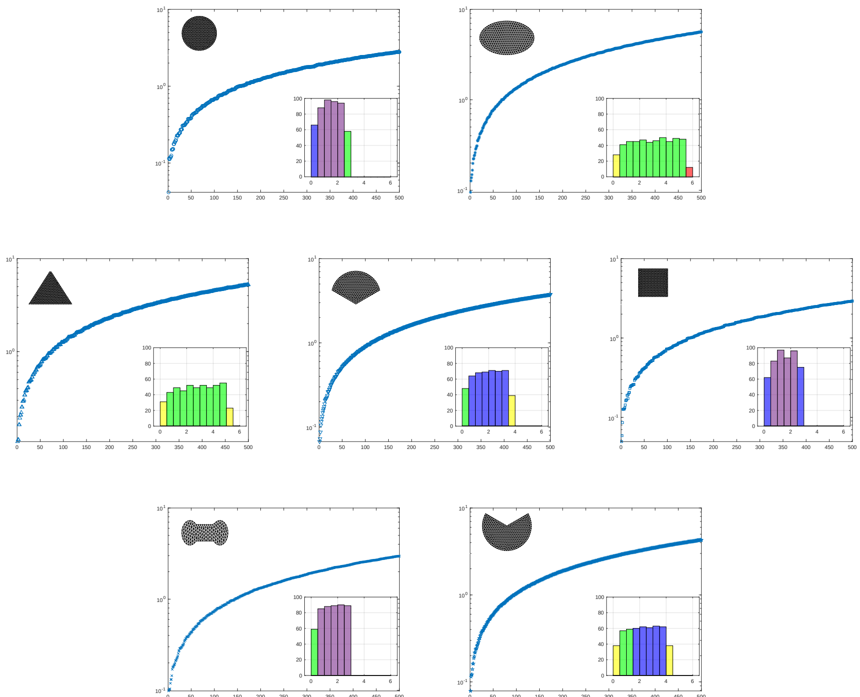

Figure 1: The distribution of 500 positive eigenvalues for all domains in case 1. The y-coordinate represents the logarithm of the eigenvalue. The histograms show the distribution of 500 positive eigenvalues in 12 subintervals of length 0.5 from 0 to 6.

Furthermore, we zoom in on the distribution of positive eigenvalues to show the first 10 positive eigenvalues for all domains in Figure 2. We also list the first positive eigenvalue for each domain in Table 3.

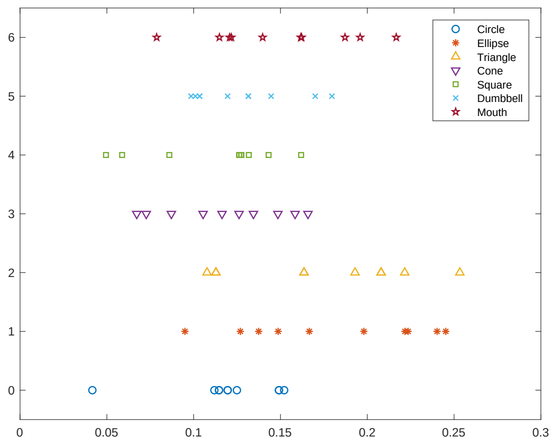

Figure 2: This figure shows the distributions of first 10 eigenvalues for different domains in case 1.

Domains	1st pos. eig.
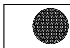	0.041644
	0.094985
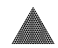	0.107700
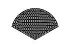	0.067220
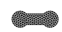	0.098504
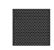	0.049478
	0.078684

Table 3: Values of first positive eigenvalues for different domains.

The graphs of the eigenvectors corresponding to the first positive eigenvalues for different domains are listed in Figire 3-5. As pointed out above, the elastic waves in **Case 1** corresponds to the acoustic waves considered in [4] and [3]. Our numerical results show that the interior transmission eigenfunctions have the similar behaviors near the singular points, namely, they vanish near the point where the interior angle is less than π and are localized near the point where the interior angle is greater than π.

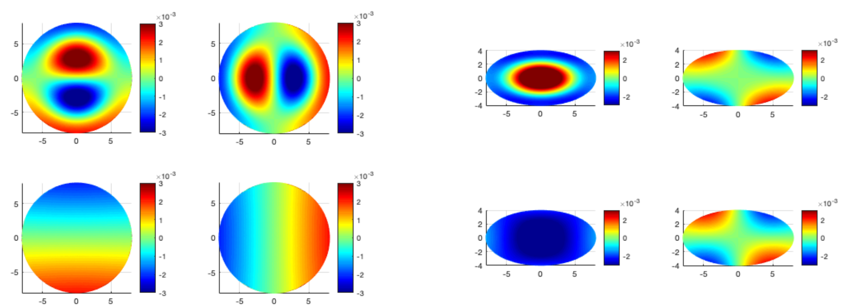

Figure 3: The interior transmission eigenfunctions associated with the first positive eigenvalues for disc and ellipse domains. The upper left, upper right, lower left, lower right subfigures correspond to u_1, u_2, v_1, and v_2, respectively.

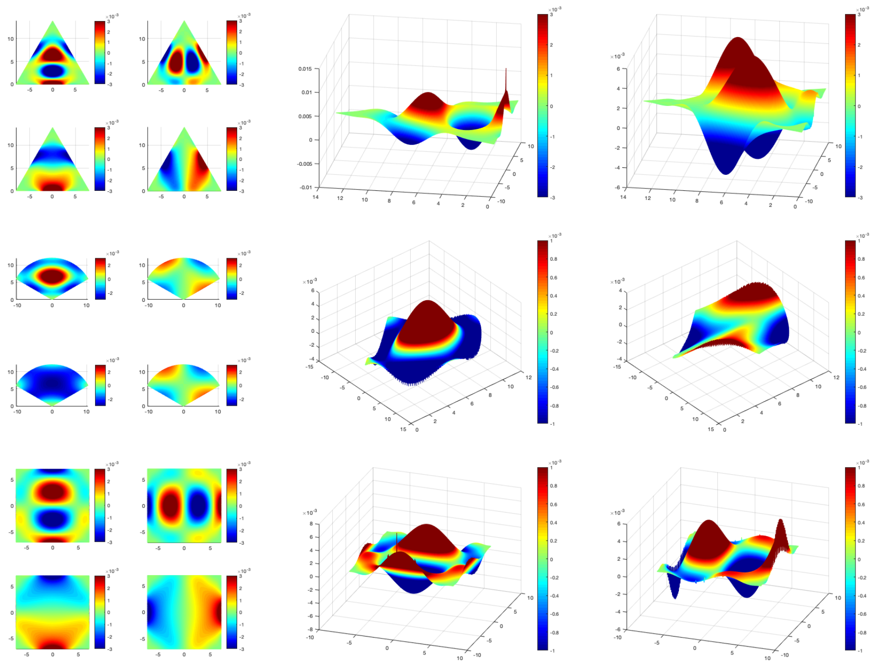

Figure 4: The interior transmission eigenfunctions associated with the first positive eigenvalues for triangle, cone, and square domains. Subfigures in first column are eigenfunctions. The upper left, upper right, lower left, lower right subfigures correspond to u_1, u_2, v_1, and v_2, respectively. Subfigures in the second and third columns are 3D plots of u_1 and u_2, respectively. We can observe that the values of u_1 and u_2 are almost zero near corners.

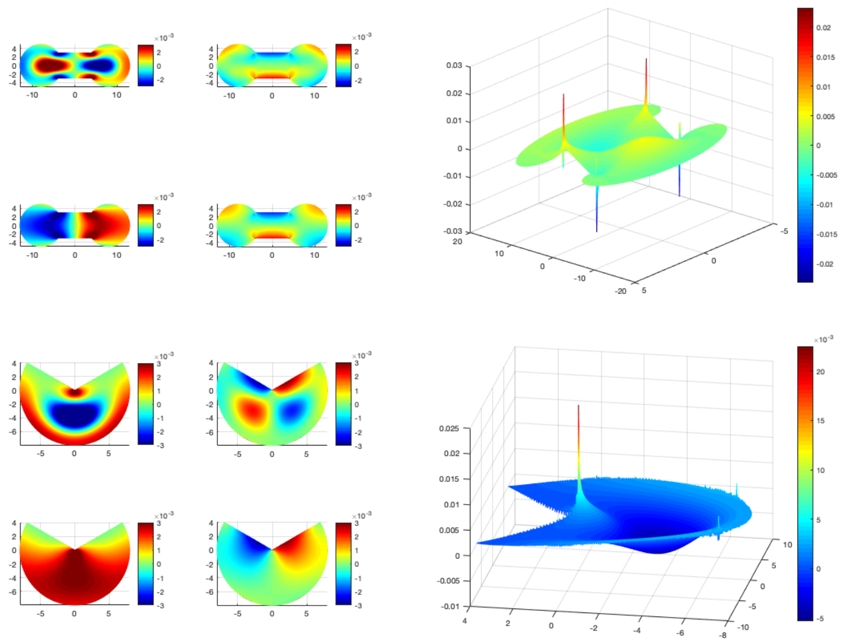

Figure 5: The interior transmission eigenfunctions associated with the first positive eigenvalues for dumbbell and mouth domains. Subfigures in first column are eigenfunctions. The upper left, upper right, lower left, lower right subfigures correspond to u_1, u_2, v_1, and v_2, respectively. Subfigures in the second column are 3D plots of u_1 for two domains. Note that the interior angles of singular points are greater than π. The localized behaviors near the singular points are clearly observed.

Case 2. For this case, we choose $\mu_0 = 200, \mu_1 = 2,\ \lambda_0 = 200, \lambda_1 = 1$ and $\rho_0 = \rho_1 = 50$. The results are shown in Figure 6.

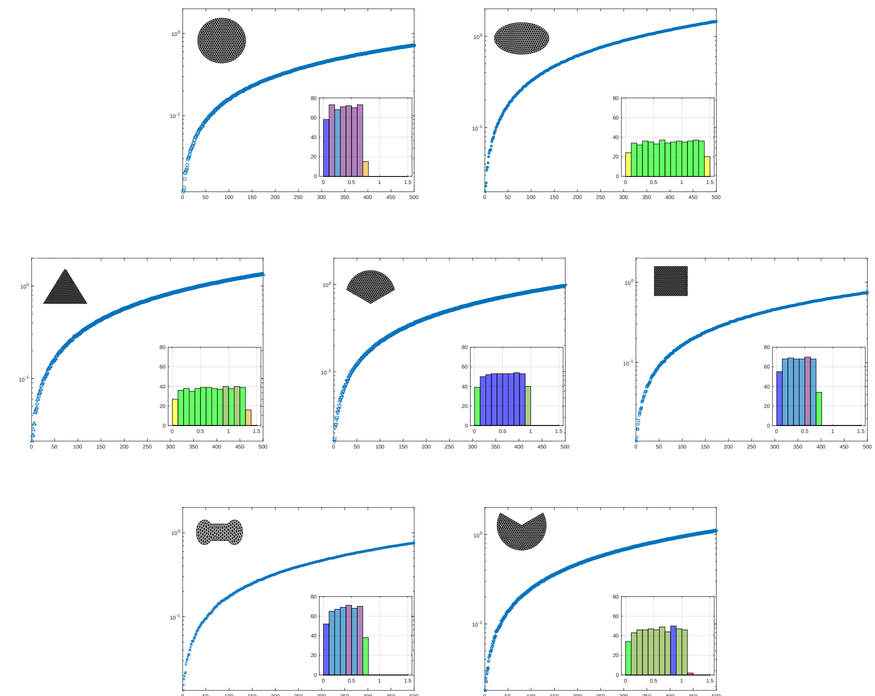

Figure 6: The distribution of 500 positive eigenvalues for all domains in case 2. The y-coordinate represents the logarithm of the eigenvalue. The histograms show the distribution of 500 positive eigenvalues in 15 subintervals of length 0.1 from 0 to 1.5.

Again, we also draw the first 10 positive eigenvalues for all domains in Figure 7. The list of the first positive eigenvalue for each domain is given in Table 4.

Like in **Case 1**, the graphs of the eigenvectors corresponding to the first positive eigenvalues for different domains are listed in Figure 8-9. Even in the acoustic wave scattering having jumps in leading order, the behaviors of interior transmission eigenfunctions near singular points have never been studied before. Our numerical simulations demonstrate some possible phenomena of interior transmission eigenfunctions near the singular points. Intuitively, since the perturbations occur at the leading order, it seems more justified to consider $\nabla \mathbf{u}$. Especially, in Figure 9, we can observe that the localization behaviors of $\nabla \mathbf{u}$ in the dumbbell and mouth domains.

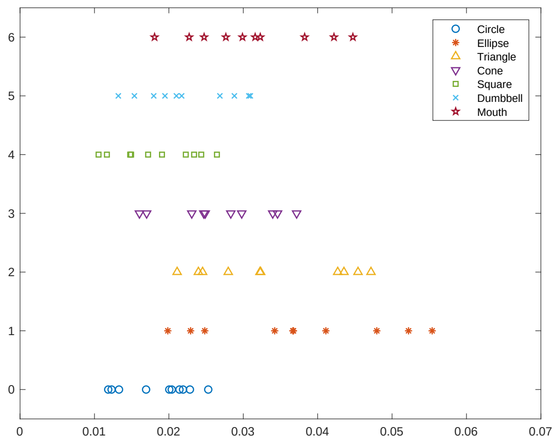

Figure 7: The distribution of first 10 eigenvalues for different domains in case 2.

Domains	1st pos. eig.
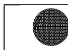	0.011849
	0.019858
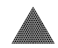	0.021110
	0.016045
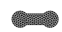	0.013208
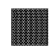	0.010552
	0.018077

Table 4: Values of first positive eigenvalues for different domains.

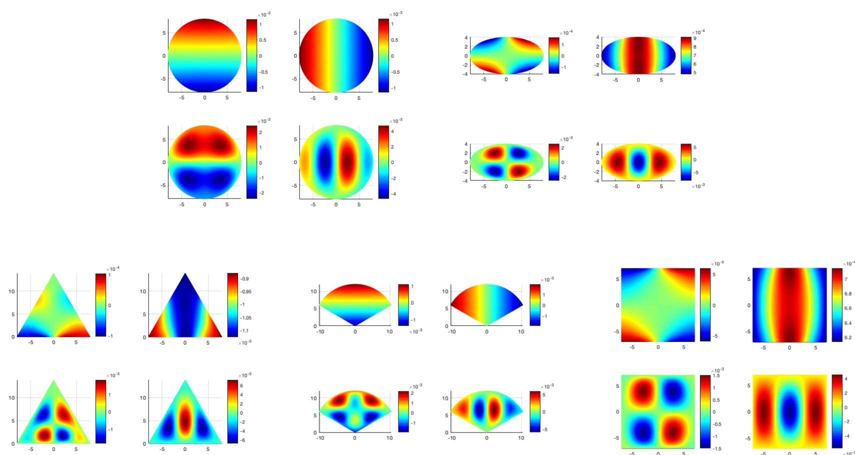

Figure 8: The interior transmission eigenfunctions associated with the first positive eigenvalues for disc, ellipse, triangle, cone, square domains. The upper left, upper right, lower left, lower right subfigures correspond to u_1, u_2, v_1, and v_2, respectively. We can observe that the interior transmission eigenfunctions $\mathbf{u}, \mathbf{v}$ in triangle, cone, square domains are almost flat near singular points.

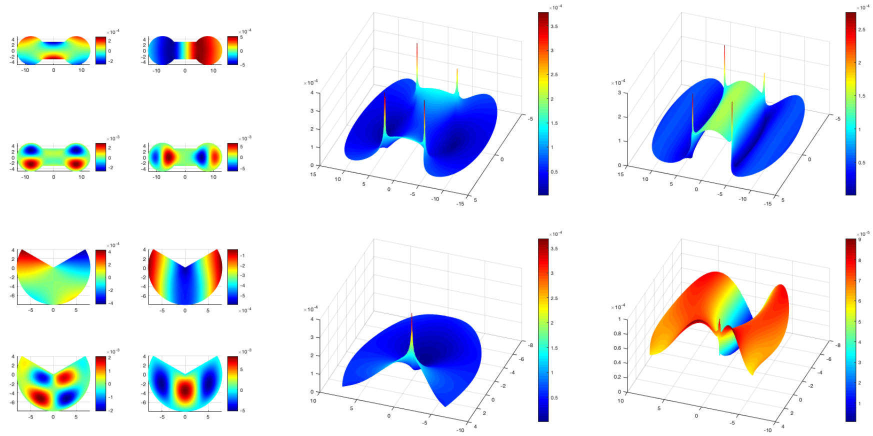

Figure 9: The interior transmission eigenfunctions corresponding to the first positive eigenvalues for dumbbell and mouth domains. The second column is the 3D plot of ∇u_1 and the third column is the 3D plot of ∇u_2. The localization behaviors are observed near the singular points.

6 Conclusions

We study the interior transmission eigenvalues for the elastic waves in this paper. We consider two cases, **Case 1**: $\mathbf{C}_0 = \mathbf{C}_1$, $\rho_0 \neq \rho_1$ and **Case 2**: $\mathbf{C}_0 \neq \mathbf{C}_1$, $\rho_0 = \rho_1$. Our aim is to propose efficient numerical algorithms to compute several hundred positive eigenvalues for both cases. After discretizing the PDEs by FEM, the problem come down to the computation of generalized eigenvalues with matrices of large size. In **Case 1**, there are a huge number of nonphysical zeros (at least $\geq m$). Finding first few positive eigenvalues from the corresponding GEP will be very ineffective. So we convert the GEP to a QEP such that all zero eigenvalues are removed. We then apply a quadratic Jacobi-Davidson to locate first 500 positive eigenvalues. The algorithm works quite efficiently.

In **Case 2**, the corresponding nonphysical eigenvalues become infinity. In view of finding first few positive eigenvalues, it seems that an algorithm for solving GEP will do the work. Unfortunately, since complex eigenvalues cloud over real eigenvalues, finding positive eigenvalues becomes ineffective. We thus used the similar idea as in **Case 1** trying to convert the GEP to a QEP. However, unlike in **Case 1**, the key matrix $\mathcal{K}$ used in this conversion is degenerate. We need to first remove the null space of $\mathcal{K}$ and convert the new GEP to a QEP. To perform the computations efficiently, it is also essential to take into account of the sparsity of the matrices in all matrix operations. As far as we can check, there is no numerical results dealing with the interior transmission eigenvalues for the elastic waves with jumps in the elasticity tensors before. The interior transmission eigenfunctions in a domain with corners exhibit interesting behaviors near corners. For the acoustic waves, there were already rigorous proofs.

In this work, we provide numerical evidences of similar phenomena near corners for the interior transmission eigenfunctions of the elastic waves. It is of course an interesting project to prove this property rigorously.

Acknowledgements

The authors would like to thank Professor Tsung-Ming Huang for many insightful discussions and for crucial helps on numerical simulations. We also want to express our gratitude to Professor Hongyu Liu for many discussions on the interior transmission eigenfunctions. The first and third authors were partially supported by MOST. The second author is supported in part by MOST, NCTS, and S T Yau Center of National Chiao Tung University.

References

[1] C. Bellis, F. Cakoni, and B. B. Guzina. Nature of the transmission eigenvalue spectrum for elastic bodies. *IMA J. Appl. Math.*, 78:895–923, 2013.

[2] C. Bellis and B. B. Guzina. On the existence and uniqueness of a solution to the interior transmission problem for piecewise homogeneous solids. *Journal of Elasticity*, 101:29–57, 2010.

[3] E. Blasten, X. Li, H. Liu, and Y. Wang. On vanishing and localization near cusps of transmission eigenfunctions: a numerical study. *Inverse Problems*, 33:105001, 2017.

[4] E. Blasten and H. Liu. On vanishing near corners of transmission eigenfunctions. *Journal of Functional Analysis*, 273(11):3616–3632, 2017.

[5] F. Cakoni and D. Colton. *Qualitative methods in inverse scattering theory: An introduction.* Springer Science & Business Media, 2005.

[6] F. Cakoni, D. Colton, P. Monk, and J. Sun. The inverse electromagnetic scattering problem for anisotropic media. *Inverse Problems*, 26(7):074004, 2010.

[7] F. Cakoni, D. Gintides, and H. Haddar. The existence of an infinite discrete set of transmission eigenvalues. *SIAM J. Math. Anal.*, 42(1):237–255, 2010.

[8] F. Cakoni and H. Haddar. On the existence of transmission eigenvalues in an inhomogeneous medium. *Appl. Anal.*, 88(4):475–493, 2009.

[9] F. Cakoni and H. Haddar. Transmission eigenvalues in inverse scattering theory. In G. Uhlmann, editor, *Inverse Problems and Applications: Inside Out II*, volume 60 of *Math. Sci. Res. Inst. Publ.*, pages 527–578. Cambridge University Press, Cambridge, 2012.

[10] A. Charalambopoulos. On the interior transmission problem in nondissipative, inhomogeneous, anisotropic elasticity. *Journal of Elasticity*, 67:149–170, 2002.

[11] A. Charalambopoulos and K. A. Anagnostopoulos. On the spectrumn of the interior transmission problem in isotropic elasticity. *Journal of Elasticity*, 90:295–313, 2008.

[12] A. Charalambopoulos, D. Gintides, and K. Kiriaki. The linear sampling method for the transmission problem in three-dimensional linear elasticity. *Inverse Problems*, 18:547–558, 2002.

[13] D. Colton and A. Kirsch. A simple method for solving inverse scattering problems in the resonance region. *Inverse Problems*, 12(4):383, 1996.

[14] D. Colton and R. Kress. *Inverse Acoustic and Electromagnetic Scattering Theory*, volume 93 of *Applied Mathematical Sciences*. Springer, New York, 3rd edition, 2013.

[15] D. Colton, P. Monk, and J. Sun. Analytical and computational methods for transmission eigenvalues. *Inverse Problems*, 26:045011, 2010.

[16] D. Colton, L. Päivärinta, and J. Sylvester. The interior transmission problem. *Inverse Probl. Imaging*, 1(1):13–28, 2007.

[17] G. C. Hsiao, F. Liu, J. Sun, and L. Xu. A coupled BEM and FEM for the interior transmission problem in acoustics. *J. Comput. Appl. Math.*, 235:5213–5221, 2011.

[18] T.-M. Huang, W.-Q. Huang, and W.-W. Lin. A robust numerical algorithm for computing Maxwell's transmission eigenvalue problems. *SIAM J. Sci. Comput.*, 37:A2403–A2423, 2015.

[19] X. Ji, P. Li, and J. Sun. Computation of transmission eigenvalues for elastic waves. *arXiv:1802.03687v1 [math.NA]*, 11 Feb 2018.

[20] X. Ji, J. Sun, and T. Turner. Algorithm 922: A mixed finite element method for Helmholtz transmission eigenvalues. *ACM Trans. Math. Software*, 38:29, 2012.

[21] X. Ji, J. Sun, and H. Xie. A multigrid method for Helmholtz transmission eigenvalue problems. *J. Sci. Comput.*, 60(2):276–294, 2014.

[22] A. Kirsch. Factorization of the far field operator for the inhomogeneous medium case and an application in inverse scattering theory. *Inverse Problems*, 15:413–429, 1999.

[23] A. Kirsch. On the existence of transmission eigenvalues. *Inverse Probl. Imaging*, 3(2):155–172, 2009.

[24] A. Kirsch and N. Grinberg. *The factorization method for inverse problems.* Number 36. Oxford University Press, 2008.

[25] A. Kleefeld. A numerical method to compute interior transmission eigenvalues. *Inverse Problems*, 29(10):104012, 2013.

[26] T. Li, T. M. Huang, W. W. Lin, and J. N. Wang. An efficient numerical algorithm for computing densely distributed positive interior transmission eigenvalues. *Inverse Problems*, 33:035009, 2017.

[27] T. Li, T. M. Huang, W. W. Lin, and J. N. Wang. On the transmission eigenvalue problem for the acoustic equation with a negative index of refraction and a practical numerical reconstruction method. *Inverse Probl. Imaging*, 12(4):1033–1054, 2018.

[28] T. Li, W.-Q. Huang, W.-W. Lin, and J. Liu. On spectral analysis and a novel algorithm for transmission eigenvalue problems. *J. Sci. Comput.*, 64(1):83–108, 2015.

[29] L. Päivärinta and J. Sylvester. Transmission eigenvalues. *SIAM J. Math. Anal.*, 40(2):738–753, 2008.

[30] J. Sun. Iterative methods for transmission eigenvalues. *SIAM J. Numer. Anal.*, 49(5):1860–1874, 2011.

[31] J. Sun and L. Xu. Computation of Maxwell's transmission eigenvalues and its applications in inverse medium problems. *Inverse Problems*, 29:104013, 2013.